

An Interpolatory Subdivision for Volumetric Models over Simplicial Complexes

Yu-Sung Chang Kevin T. McDonnell Hong Qin

Department of Computer Science
State University of New York at Stony Brook
{yusung|ktm|qin}@cs.sunysb.edu

Abstract

Subdivision has gained popularity in computer graphics and shape modeling during the past two decades, yet volumetric subdivision has received much less attention. In this paper, we develop a new subdivision scheme which can interpolate all of the initial control points in 3D and generate a continuous volume in the limit. We devise a set of solid subdivision rules to facilitate a simple subdivision procedure. The conversion between the subdivided mesh and a simplicial complex is straightforward and effective, which can be directly utilized in solid meshing, finite element simulation, and other numerical processes. In principle, our solid subdivision process is a combination of simple linear interpolations in 3D. Affine operations of neighboring control points produce new control points in the next level, yet inherit the original control points and achieve the interpolatory effect. A parameter is offered to control the tension between control points. The interpolatory property of our solid subdivision offers many benefits which are desirable in many design applications and physics simulations, including intuitive manipulation on control points and ease of constraint enforcement in numerical procedures. We outline a proof that can guarantee the convergence and C^1 continuity of our volumetric subdivision and limit volumes in regular cases. In addition to solid subdivision, we derive special rules to generate C^1 surfaces as B-reps and to model shapes of non-manifold topology. Several examples demonstrate the ability of our subdivision to handle complex manifolds easily. Numerical experiments and future research suggestions for extraordinary cases are also presented.

1. Introduction and Background

Subdivision offers an effective way to represent geometric shapes such as curves and surfaces. It has been researched for more than 20 years since the early pioneer-

ing work by Catmull and Clark [2]. To date, it has stimulated ever-increasing interest in both theoretical and practical aspects. In essence, the success of subdivision is primarily because of its simplicity and ease of use. A subdivision process in its simplest form can be essentially expressed as successive affine combinations from the coarser to the finer step, i.e.,

$$p' = Sp,$$

where S is a subdivision matrix whose entries represent all the subdivision rules (i.e., affine operations). By successively introducing new vertices, we hierarchically refine a mesh and acquire a desired shape in the limit. In many cases, the limit shape is of well-known form, for instance, B-spline or Box spline [2, 12, 16, 3]. However, they oftentimes result in an *approximate* scheme that does not guarantee a geometric invariant of control points in subsequent levels. It may be noted that most of subdivision schemes are based on edge bisection, which introduces 4 new cells for each triangle or quadrilateral. Kobbelt [10] suggests a subdivision scheme based on a tiling scaled by the factor $\sqrt{3}$. Velho's 4-8 subdivision [16] utilizes 4.8^2 tiling to generate Box splines. They both result in a gradual approach to the limit surface.

1.1. Interpolatory Subdivision

Dyn *et al.* [6, 7] have intensively investigated interpolatory subdivision schemes and their variations. Unlike the approximate subdivision rules, these schemes *interpolate* the initial control points, which permit points to be geometrically fixed in subsequent levels. Dyn *et al.* [5] derive a series of interpolatory schemes for surfaces using generating functions, averaging, and tensor products, and give detailed analyses of their convergence on a regular grid. Note that, it is relatively easier to enforce constraints in any interpolatory scheme because of its invariant property. Therefore, it is more suitable for finite element analysis, physics-based simulation, etc. One key motivation for this work is to de-

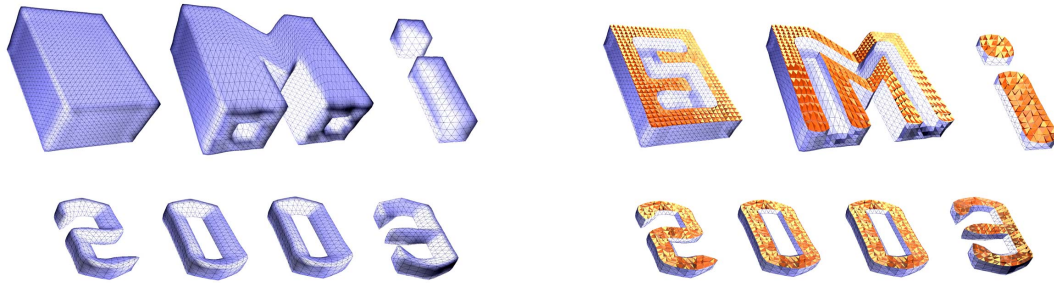


Figure 1. SMI logo and its cross-section created using our interpolatory subdivision scheme for solids. The new scheme successfully models complex structures inside the solid. It can also handle non-trivial topology with ease. Note that, throughout this paper the boundary of solid models is colored blue, and the cross-section of solid models is colored yellow.

velop a novel subdivision scheme for solid models that can interpolate all the control points scattered in 3D.

1.2. Subdivision Analysis

Since Doo and Sabin’s work [4], there has been much progress in analysis of subdivision schemes. Mostly, the analysis has been concentrated on extraordinary cases. Much literature [15, 17, 19] demonstrates proofs of continuity of various schemes, mainly based on spectral analysis techniques. Reif [15] discusses the necessary and sufficient conditions of continuity around extraordinary vertices using characteristic maps and spectral analysis. Dyn *et al.* [8] detail a similar proof for interpolatory schemes on regular meshes.

1.3. Volume Subdivision

Despite the popularity of subdivision, there has been less research regarding volumetric subdivision, i.e., subdivision solids. MacCracken *et al.* [13] propose a tensor-product extension of Catmull-Clark subdivision in the volumetric setting, mainly for the purpose of free-form deformation in 3D space. Later on, Bajaj *et al.* [1] further extended the scheme with analysis based on numerical experiments. Their approach is interesting because it can be utilized to generate non-manifold meshes. Most recently, Chang *et al.* [3] suggest non-tensor-product based subdivision over tetrahedral meshes whose limit solid is a trivariate Box spline. Additionally, Peters *et al.* [14] use 7-directional trivariate Box splines to blend CSG primitives. It may be noted that stationary subdivision generally has problems which are more apparent in interpolatory schemes. Kobbelt *et al.* [11] summarize variational subdivision schemes which minimize fairness functionals during the subdivision process. Weimer

and Warren [18] suggest variational schemes whose limits are solutions for certain Partial Differential Equations (PDEs).

1.4. Research Contribution

In this paper, we devise a novel interpolatory subdivision scheme for volumetric models that can be decomposed into simplicial complexes. We choose the octet-truss as our underlying mesh, which consists of two types of polyhedra, i.e., tetrahedra and octahedra. Note that, this mesh can be converted into a simplicial complex in an efficient way and vice versa. This offers the benefit of generating a tetrahedral mesh, which is more desirable in many finite element applications. The rule is based on simple connectivity information and affine combinations with tension control by means of a weight. Our scheme is C^1 , stationary, interpolatory, and based on edge-bisection. In light of its interpolatory aspect, the scheme has several key advantages including:

- it is straightforward to enforce constraints during physics-based simulation,
- it supports intuitive, direct manipulation of control points,
- there is no need for an auxiliary subdivision matrix for vertex points, and
- it is not necessary for subdivision matrix inversion during data fitting applications.

Meanwhile, it also inherits many attractive properties of existing subdivision schemes such as:

- multiresolution analysis and levels of detail,
- numerical efficiency and stability,
- arbitrary topology or genus, and

- simplicity in implementation.

In the remainder of this paper, after detailing the subdivision rules of our new interpolatory volumetric subdivision over simplicial complexes, we also give an outline of its convergence analysis and a proof of its C^1 continuity for regular meshes. We then document numerical results on irregular cases. Finally, we present several examples that demonstrate the modeling potential of our generalized rules to represent shapes with creases and of non-manifold topology.

2. Subdivision Rules

This section details our new subdivision rules.

2.1. The Mesh and the Mask

One of our goals in this paper is to develop an interpolatory subdivision scheme whose underlying domain for control meshes is a simplicial complex. In 3D, it implies that a control mesh should be a collection of tetrahedra. There are several benefits of having a simplicial complex as an underlying mesh. One of the benefits is the fact that each face of the cells is also a simplex in a lower dimension. In our case, faces are triangles, as opposed to the quadrilaterals that appear in hexahedral meshes. This avoids the ambiguity problem that occurs in hexahedral meshes during the triangulation of models. Also, a tetrahedral mesh is frequently desirable in many finite element analysis and physics-based simulation applications.

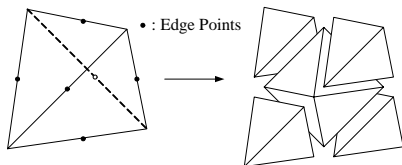


Figure 2. A simple split of a tetrahedron. It splits into 4 tetrahedra and an octahedron.

Nevertheless, a simple tetrahedral mesh lacks certain important properties that are required for the domain of a stationary subdivision scheme. One important issue is self-reproductivity. If we simply split a tetrahedron by bisecting its edges, an octahedron occurs inside (see Figure 2). This suggests multiple ways of splitting it into tetrahedra. The algorithm therefore requires a careful and complicated bookkeeping task to unify the splits in the whole process so that the finer level bears the same connectivity as the coarser level. It also proliferates extraordinary topologies,

since arbitrarily chosen tetrahedra will propagate extraordinary edges in the structure. Instead, we use octahedra as the secondary primitive and keep them during the subdivision, along with information of the *major diagonal*, which is a predefined direction for splitting during the process.

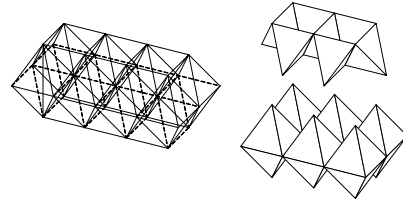


Figure 3. A typical example of an octet-truss mesh. It is comprised of an octahedral grid with tetrahedra in between.

The resulting domain forms the structure called an *octet-truss* (Figure 3), which is well-known in many research fields. In this way, it can easily maintain the regularity of the structure as well as simplify the analysis of the scheme. Moreover, we can quadrisect octahedra by major diagonals at the desired level to get a mesh that consists of tetrahedra only, if required (see Figure 4).

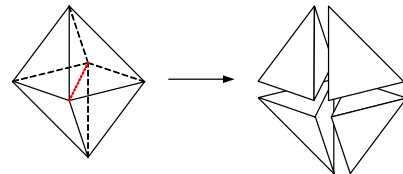


Figure 4. An octahedron can be quadrisected into tetrahedra. The red dotted line represents the major diagonal.

During the subdivision process, tetrahedral cells split into 4 tetrahedra and an octahedron, and octahedral cells split into 8 tetrahedra and 6 new octahedra. Figure 5 shows that an octahedron splits into several sub-cells in subsequent levels.

For each edge, we need information from its neighbors to calculate a new point. *One-neighbors* denote the vertices of cells sharing the given edge that are not the end points of the edge (see Figure 6(a)). *Two-neighbors* means the vertices of cells adjacent to one-neighbors that do not belong to one-neighborhood (see Figure 6(b)). When finding the neighbors, we consider an octahedron as 4 sets of tetrahe-

dra (see Figure 4) and apply the same rules as for tetrahedral cases.

2.2. The Rules

The subdivision process can be essentially understood as a linear interpolation with perturbation. To linearly interpolate two points p_0 and p_1 , we can successively introduce a bisector of segments, i.e.,

$$p' = \frac{1}{2}(p_0 + p_1)$$

in each subdivision step. We introduce perturbation using information from its neighbors,

$$p' = \frac{1}{2}(p_0 + p_1) + f(w, \bar{q}, \bar{r}),$$

where \bar{q} and \bar{r} are *one-neighbors* and *two-neighbors*, respectively. The weight w controls the tension between control points. We choose $w \in [0, \frac{1}{8})$ to assure the convergence, which is explained in Section 4. When $w = 0$ the subdivision is simply mesh refinement by edge bisection. We choose a linear function f in our case. More specifically, we categorize new points which are introduced in the next level of subdivision as vertex, edge, and cell points and devise rules for each case.

2.2.1. Vertex Points Since our scheme is interpolatory, it is obvious that a vertex point is geometrically invariant in each level. Therefore, if p^k is a point in a subdivision level k , a vertex point v^{k+1} at level $k + 1$ is simply assigned by

$$v^{k+1} = p^k. \quad (1)$$

2.2.2. Edge Points A new edge point can be written as three parts of affine combinations, or as a weighted average of two end points that define the edge, one-neighbors, and two-neighbors. In the regular case (see Figure 7), the number of one-neighbors and two-neighbors are both 6. Therefore, we can express

$$e^{k+1} = \frac{1}{2}(p_0^k + p_1^k) + w \sum_{i=0}^5 q_i^k - w \sum_{j=0}^5 r_j^k, \quad (2)$$



Figure 5. An octahedron splits into sub-cells during the subdivision process.

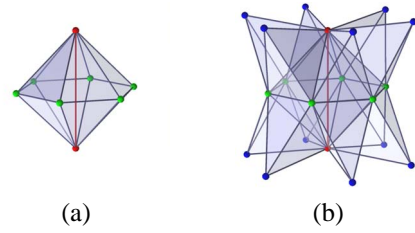


Figure 6. Neighbors of an edge. (a) Green vertices denote one-neighbors. The edge is colored in red. (b) Blue vertices denote two-neighbors. They consist of the vertices from adjacent cells of one-neighbor cells.

where q_i and r_i are one-neighbors and two-neighbors, respectively. In a more general case, we shall average them by the number of their neighbors, i.e.,

$$e^{k+1} = \frac{1}{2}(p_0^k + p_1^k) + \frac{M}{N}w \sum_{i=0}^{N-1} q_i^k - w \sum_{j=0}^{M-1} r_j^k, \quad (3)$$

where N and M are the numbers of one-neighbors and two-neighbors, respectively. It should be noted that Equation (3) only ensures convergence around irregular vertices. There is a slight, however noticeable, degeneracy when a vertex has valence of 4, which rarely occurs in a real-world model.

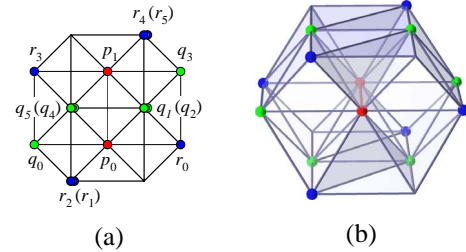


Figure 7. Neighbors of an edge in the regular case. We treat octahedral cells as 4 tetrahedra. Green and blue vertices denote one-neighbors and two-neighbors, respectively. (a) A top view of the mask. The thicker lines indicate the higher layers. Unfilled circles denote vertices in the lower layer. (b) The mask in 3D view.

2.2.3. Cell Points A cell point occurs during a split of an octahedron. Since we maintain the major diagonal, the rule can be considered as an edge rule applied on the major diagonal shown in Figure 8(a). In this situation, we can ex-

press a cell point c^{k+1} at level $k + 1$ as

$$c^{k+1} = \frac{1}{2}(p_0^k + p_1^k) + w \sum_{i=0}^5 q_i^k - w \sum_{j=0}^5 r_j^k. \quad (4)$$

Because of the size of the edge mask, it is relatively difficult to apply it directly on the mesh, especially when an extraordinary case occurs. We devise a modified mask (see Figure 8(b)) which is easier to apply in general. The continuity around this particular setting is discussed in Section 4.

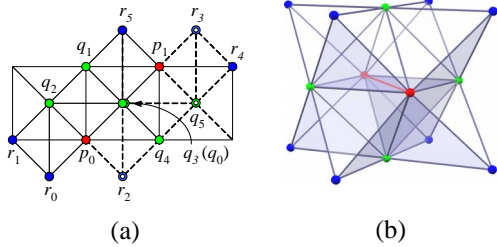


Figure 8. Cell point rules. (a) A direct application of the edge mask over a major diagonal (top view). The thicker lines and dotted lines indicate the higher and lower layers, respectively. Unfilled circles denote vertices in the lower layer. (b) Modified cell mask.

2.3. Special Cases

Not only extraordinary cases but also the boundary and neighbors of boundary all need special care. In the interest of simplicity, we choose Dyn’s Butterfly scheme [7] for the boundary representation. In addition, there is the necessity of devising special rules for neighbors of the boundary, since they only have a portion of the neighbors required to apply the aforementioned rules. As noted and derived in [20], even the boundary/crease/extraordinary rules for a surface are more complex than one can do justice in a single paper. It is particularly troublesome in our scheme due to the large mask sizes. We choose edge bisectors without any weight for these edge points and only restrict ourselves in simple cases so that such cases result in minimal deformation.

3. Experimental Results

Figures 13, 14, and 15 show several examples which have non-trivial topologies and are oftentimes impossible to generate as a single object by using surface subdivision

schemes (also refer to Figure 1 and Color Plate). In Figure 16, we use a sweeping curve equation with a specially designed mesh to generate a spiral model. Figure 17 and 18 (see also Color Plate) demonstrates the ability of our new subdivision scheme to handle non-manifold topology models without having to introduce a special set of rules. Not only does the scheme successfully display the solid part (which is colored in orange), it also has no difficulty in processing the surface-only region, which is colored in purple (see Figure 17 and Color Plate). The rule also can be applied to the degenerating case (see Figure 18 and Color Plate) without a significant modification. In addition, the scheme is also able to define the transition between two different regions. The weight for most of the results reported in this paper is $w = \frac{1}{16}$, unless otherwise documented. Besides the shape modeling functionality, our novel interpolatory subdivision scheme can also be readily suitable for many other solid modeling applications, including:

Direct Manipulation In contrast to an approximate scheme, changes on control points directly affect the modeled shape (see Figure 19). As a result, this can offer a naïve user more intuitive interaction between control points and a desired model.

Material Representation Besides shape geometry, we can also assign material properties to control points and apply exactly the same subdivision rules on the control mesh to acquire smoothly interpolated properties. We refer to Color Plate for examples of the model with color information associated with control points. The colors between control points are continuously interpolated through the use of our subdivision rules.

Tension Control By controlling the weight w , we will have different effects on the geometry of our models. In the case of $w = 0$ (see Figure 12(a)), the subdivision simply performs a linear interpolation. By increasing w , we expect to receive many ripples in a model. Eventually, the subdivision diverges if w exceeds a certain threshold (see Figure 12(f)).

Let us briefly compare our new solid subdivision scheme with other approximate schemes. In particular, consider the approximate scheme recently proposed by Chang *et al.* [3]. Figure 9 demonstrates how these two schemes differ for the same initial control mesh. As shown in Figure 19, a user can directly change a model by modifying control points. To enforce constraints or to perform data fitting, the approximate scheme oftentimes requires the time-consuming computation of assembling the subdivision matrix and explicitly calculating its inverse, which the interpolatory scheme does not need in most cases. In addition, because of the fact that vertex points are control points from the previous level, the interpolatory scheme requires less memory than the approximate one.

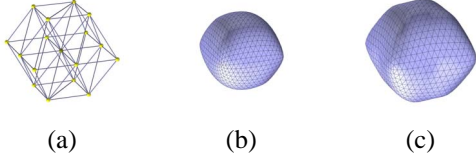


Figure 9. A comparison between an approximate scheme and the proposed interpolatory scheme. (a) The original control points. (b) Subdivision at level 4 by the approximate scheme [3]. (c) Subdivision at level 4 by the interpolatory scheme.

4. Analysis

This section briefly discuss the issues of convergence and continuity of our new scheme.

4.1. The Continuity on Regular Topology

Suppose that the scheme is expressed in matrix form, $p' = Sp$. It is relatively straightforward to confirm that the scheme is convergent by means of eigenvalue analysis of S . In particular, the subdominant eigenvalue of S is strictly less than 1 for $w < \frac{1}{8}$, which is sufficient to show the convergence of our interpolatory scheme. To prove the continuity of the limit solid on regular topology, however, we must investigate its generating function [17, 8]. In principle, any binary stationary subdivision scheme for solids can be written as

$$P_{k+1}(z) = a(z)P_k(z^2), \quad z \in \mathbb{R}^3, \quad (5)$$

where $P_k(z) = \sum_{\mu \in \mathbb{Z}^3} p_\mu^k z^\mu$ is a formal generating function associated with the control points $p^k = \{p_\mu^k\}_{\mu \in \mathbb{Z}^3}$ at level k , and $a(z)$ is the characteristic polynomial derived from the subdivision matrix S :

$$a(z) = \sum_{\mu \in \mathbb{Z}^3} a_\mu z^\mu. \quad (6)$$

Comparing these coefficients with n iterations of subdivision process, one can derive [8]

$$\|S^n\|_\infty = \max_{\gamma} \sum_{\nu \in \mathbb{Z}^3} a_{2^n \nu + \gamma}^{[n]}, \quad (7)$$

where $\gamma \in \{0, 1, \dots, 2^n - 1\}^3$ and $a^{[n]}(z) = \prod_{j=0}^{n-1} a(z^{2^j}) = \sum_{\mu} a_\mu^{[n]} z^\mu$. We now use the special case of the following theorem [8] to prove the continuity of our scheme.

Theorem. Let the characteristic polynomial of S be the form

$$a(z) = q(z) \prod_{i=1}^s (z^{\theta^{(i)}} + 1), \quad (8)$$

where q is a Laurent polynomial and $\theta^{(i)} \in \mathbb{Z}^s$ satisfies

$$|\det(\theta^{(1)}, \dots, \theta^{(s)})| = 1. \quad (9)$$

Let D_i be the subdivision matrix corresponding to the polynomial $a(z)(z^{\theta^{(i)}} + 1)^{-1}$. Then the subdivision scheme associated with S is uniformly convergent if and only if for some $L \in \mathbb{Z}_+$

$$\|D^L\|_\infty = \max_{1 \leq i \leq s} \|D_i^L\|_\infty < 1. \quad (10)$$

The characteristic polynomial of our new scheme has the form of

$$a(z) = \sum_{\mu \in \mathbb{Z}^3} a_\mu z^\mu. \quad (11)$$

To obtain the coefficients, we investigate our subdivision masks over a regular grid \mathbb{Z}^3 . For instance, Figure 10 explains how to acquire coefficients associated with an edge, in this case, from $(-1, 0, 0)$ to $(1, 0, 0)$. We perform the same process over each edge $\overline{p_{2k} p_{2k+1}}$, $k = 0, \dots, 6$, where $p_0(-1, 0, 0)$, $p_1(1, 0, 0)$, $p_2(0, -1, 0)$, $p_3(0, 1, 0)$, $p_4(0, 0, -1)$, $p_5(0, 0, 1)$, $p_6(-1, -1, -1)$, $p_7(1, 1, 1)$, $p_8(-1, 0, -1)$, $p_9(1, 0, 1)$, $p_{10}(0, -1, -1)$, $p_{11}(0, 1, 1)$, $p_{12}(-1, -1, 0)$, and $p_{13}(1, 1, 0)$. The coefficient is explicitly formulated as

$$a_\mu = 1, \quad \mu = (0, 0, 0)$$

$$a_\mu = \frac{1}{2}, \quad \mu = (\pm 1, 0, 0) \\ = (1, 1, 1), (-1, -1, -1) \\ = (1, 1, 0), (-1, -1, 0)$$

$$a_\mu = w, \mu = (2, 1, 2), (-2, -1, -2) \\ = (2, 1, 1), (-2, -1, -1) \\ = (2, 1, 0), (-2, -1, 0) \\ = (2, 1, -1), (-2, -1, 1) \\ = (1, 1, -1), (-1, -1, 1) \\ = (1, -1, 0)$$

$$a_\mu = -w, \mu = (3, 2, 1), (-3, -2, -1) \\ = (3, 1, 1), (-3, -1, -1) \\ = (3, 1, 0), (-3, -1, 0) \\ = (2, 3, 2), (-2, -3, -2) \\ = (2, -1, 0), (-2, 1, 0) \\ = (2, -1, -1), (-2, 1, 1)$$

Finally, we have

$$a_{\mu'} = a_\mu, \text{ if } \mu' = \sigma(\mu), \quad \sigma \in S_3,$$

where S_3 denotes the set of all permutations over $\{1, 2, 3\}$, which is followed by the symmetry of the subdivision mask

in the regular case. The function can be factored using $(1+z_1)(1+z_2)(1+z_3)(1+z_1z_2z_3)$. Therefore, it can be written as

$$a(z) = \frac{1}{2}(z_1z_2z_3)^{-1}p(z) \prod_{i=1}^4 (1+z^{\theta^{(i)}}) \quad (12)$$

$$\{\theta^{(i)}\} = \{(1,0,0), (0,1,0), (0,0,1), (1,1,1)\}, \quad (13)$$

where $p(z)$ is a Laurent polynomial with respect to z_1 , z_2 , and z_3 which is of the form $p(z) = 1 - wq(z_1, z_2, z_3)$. If $w = 0$, Equation (12) becomes the generating function of a linear interpolation.

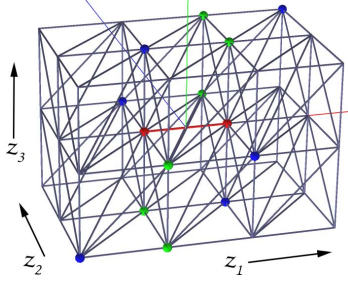


Figure 10. An example of coefficients for the generating function. Red, green, and blue vertices have associated coefficients of $\frac{1}{2}$, w , and $-w$, respectively.

To prove that the scheme is C^1 , it is sufficient to show that $\|D_{(i_1, i_2)}^L\| < 1$ and $\|D_{i_1}^L\| < 1$, $i_1 \neq i_2$ for some L where

$$\begin{aligned} D_{(i_1, i_2)}(z) &= 2(1+z_{i_1})^{-1}(1+z_{i_2})^{-1}a(z) \\ D_{i_1}^L(z) &= 2(1+z_{i_1})^{-1}(1+z_1z_2z_3)^{-1}a(z). \end{aligned}$$

Because $a(z)$ is invariant for a permutation on indices, it is equivalent to show $\|D_{(1,2)}^L\| < 1$ and $\|D_1^L\| < 1$ where

$$\begin{aligned} D_{(1,2)}(z) &= 2(1+z_1)^{-1}(1+z_2)^{-1}a(z) \\ D_1^L(z) &= 2(1+z_1)^{-1}(1+z_1z_2z_3)^{-1}a(z), \end{aligned}$$

respectively.

It has been proven numerically that $\|D_{(1,2)}^L\| < 1$ and $\|D_1^L\| < 1$ for $w = \frac{1}{16}$, especially when $L > 5$. In more general cases, the conditions are satisfied for some L , if $w > 0$ is small enough.

4.2. The Continuity over Irregular Topologies

Unlike surface subdivision schemes whose irregular analysis involves only extraordinary vertices, we must take care of both extraordinary vertices and edges in

solid schemes [1]. Unfortunately, existing spectral analysis using Discrete Fourier Transform (DFT) [4, 19] cannot be directly adopted for solid schemes, as the technique is based on spectral behavior over a 2-dimensional domain. However, we can still employ eigenvalue and characteristic map analysis [15] numerically, at least for restricted cases, which are well-understood techniques for surface subdivision analysis.

For instance, local subdivision matrices S of the scheme around extraordinary vertices and edges satisfy an eigenvalue property of

$$\lambda_0 = 1 \gneq \lambda_1 \geq \lambda_2 \geq \lambda_3 \gneq \lambda_4, \dots, \lambda_n, \quad (14)$$

where λ_i 's are eigenvalues of A in decreasing order. It is worth mentioning that we have triple subdominant eigenvalues which are strictly less than 1. Also, we have numerically generated characteristic maps from those eigenvalues and associated eigenvectors as their control nets, and have confirmed that the maps are one-to-one and regular over a large number of iterations. Some of examples are shown in Figure 11.

Even though we can confirm the regularity of the characteristic map for each specific case, it is impossible to prove it symbolically due to the aforementioned reason (i.e., DFT is not applicable in volumetric settings). In general, extraordinary edge cases are limited and simple to generate. However, the number of extraordinary vertex cases is exponentially bounded by the vertex valence n and is associated with the number of triangulation of n points (in general position) over a spherical domain [9]. Further research should be conducted to exploit a more systematic way in order to prove extraordinary cases in solid subdivision schemes. Such an investigation might result in a new spectral analysis tool for even higher domains.

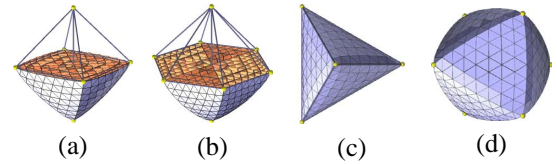


Figure 11. Control nets for rings of characteristic maps for our scheme. (a-b) Control nets for extraordinary edges with 4 and 6 incident vertices, respectively (cross-sections). (c-d) Control nets for extraordinary vertices of valence 4 and 6, respectively.

5. Conclusions and Future Work

We have presented a new interpolatory subdivision scheme for volumetric models which inherits many benefits of other interpolatory subdivision surfaces. Among many advantages for shape modeling, ease of constraint enforcement and intuitive control point manipulation are two key features, which have been shown in examples above. The underlying octet-truss mesh offers the compatibility with other existing meshes, including different types of commonly-used finite element functions. In contrast to surface subdivision schemes, our new solid scheme can handle complex structures inside models and treat non-manifold topologies easily without having special rules. Moreover, the scheme can represent material properties associated with control points and interpolate them smoothly. The proof of C^1 continuity has been given briefly, which ensures the quality of limit solids.

Even though we have outlined the convergence and continuity analysis for our scheme, most of questions involving irregular cases are still open and under-explored in general. In particular, the lack of a proper analysis tool has hindered the authors from performing symbolic spectral analysis for general cases. Due to this fact, our scheme is unable to guarantee a higher order of continuity across extraordinary vertices and edges. Further research should be followed after this paper to address these issues. In addition, other applications utilizing the new scheme should be pursued, including data fitting, conversion from existing volumetric data, interactive modeling, and more effective and robust modeling techniques for non-manifold geometry of arbitrarily complicated topology.

Acknowledgments

This research was supported in part by the NSF ITR grant IIS-0082035, the NSF grant IIS-0097646, Alfred P. Sloan Fellowship, and Honda Initiation Award.

References

- [1] C. Bajaj, J. Warren, and G. Xu. A subdivision scheme for hexahedral meshes. *The Visual Computer*, 18:343–356, 2002.
- [2] E. Catmull and J. Clark. Recursively generated B-spline surfaces on arbitrary topological meshes. *Computer-Aided Design*, 10:350–355, Sept. 1978.
- [3] Y.-S. Chang, K. T. McDonnell, and H. Qin. A new solid subdivision scheme based on box splines. In *Proceedings of Solid Modeling 2002*, pages 226–233, 2002.
- [4] D. Doo and M. Sabin. Behaviour of recursive division surfaces near extraordinary points. *Computer-Aided Design*, 10(6):356–360, Sept. 1978.

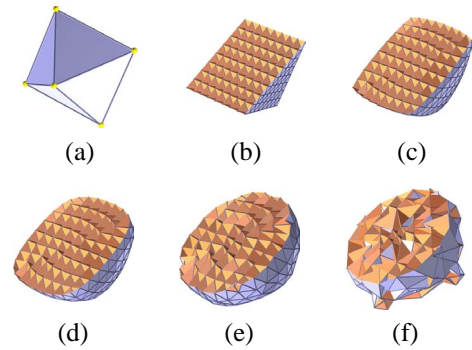


Figure 12. Tension control. (a) The original control points. (b-f) show the model at level 4 with $w = 0$, $w = \frac{1}{32}$, $w = \frac{1}{16}$, $w = \frac{1}{8}$, and $w = \frac{1}{4}$, respectively.

- [5] N. Dyn, S. Hed, and D. Levin. Subdivision schemes for surface interpolation. In A. C. *et al.*, editor, *Proceedings of the 1993 Workshop on Computational Geometry*, pages 97–118. World Scientific Publications, 1993.
- [6] N. Dyn, D. Levin, and J. Gregory. A four-point interpolatory subdivision scheme for curve design. *Computer Aided Geometric Design*, 4(4):257–268, 1987.
- [7] N. Dyn, D. Levin, and J. Gregory. A butterfly subdivision scheme for surface interpolation with tension control. *ACM Transactions on Graphics*, 9(2):160–169, April 1990.
- [8] N. Dyn and C. A. Micchelli. Using parameters to increase smoothness of curves and surfaces generated by subdivision. *Computer Aided Geometric Design*, 7:129–140, 1990.
- [9] J. O. Jacob E. Goodman, editor. *Handbook of Discrete and Computational Geometry*. CRC, 1997.
- [10] L. Kobbelt. $\sqrt{3}$ -subdivision. In *SIGGRAPH 2000 Computer Graphics Proceedings, Annual Conference Series*, pages 103–112, 2000.
- [11] L. Kobbelt and P. Schröder. A multiresolution framework for variational subdivision. *ACM Transactions on Graphics*, 17(4):209–237, 1998.
- [12] C. Loop. Smooth subdivision surfaces based on triangles. Master’s thesis, University of Utah, Dept. of Math., 1987.
- [13] R. MacCracken and K. I. Joy. Free-Form deformations with lattices of arbitrary topology. In *SIGGRAPH ’96 Computer Graphics Proceedings, Annual Conference Series*, pages 181–188, Aug. 1996.
- [14] J. Peters and M. Wittman. Box-spline based CSG blends. In *Proceedings of Solid Modeling ’97*, pages 195–206, 1997.
- [15] U. Reif. A unified approach to subdivision algorithms near extraordinary vertices. *Computer Aided Geometric Design*, 12:153–174, 1995.
- [16] L. Velho. 4-8 factorization of quadrilateral subdivision. In *Proceedings of Solid Modeling 2001*, page 303, 2001.
- [17] J. Warren and H. Weimer. *Subdivision Methods for Geometric Design: A constructive Approach*. Morgan Kaufmann Publisher, 2001.

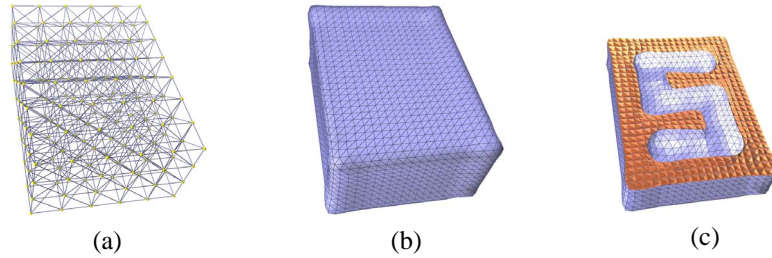


Figure 13. An embedded character. (a) The original control points. (b) The boundary of the model at level 3. (c) The cross-section of the model which reveals the “S” due to the vacancy inside the box.

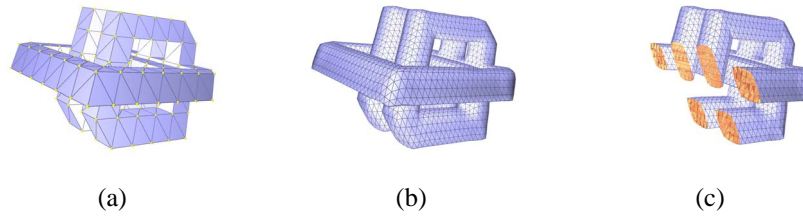


Figure 14. A knot-shaped model that has complex topology. (a) The original control points. (b) The boundary of the model at level 3. (c) A cross-section of the model.

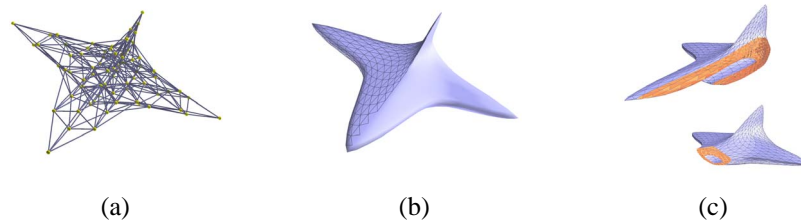


Figure 15. A simple design for space shuttle using our subdivision tools. (a) The original control points. (b) The boundary of the model at level 3. (c) Cross-sections of the model.

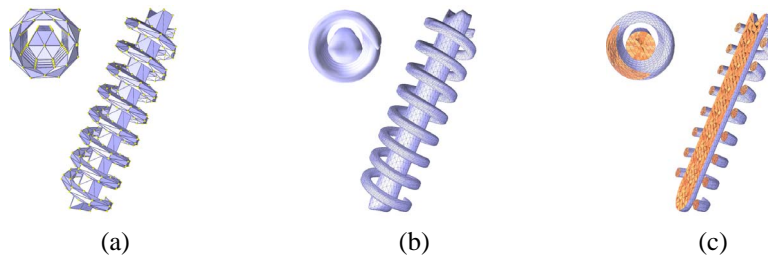


Figure 16. The scheme can be used to design a practical model such as a spiral. (a) The original control points. (b) The boundary of the model at level 3. (c) Cross-sections of the model.

[18] H. Weimer and J. Warren. Subdivision schemes for fluid flow. In *SIGGRAPH '99 Computer Graphics Proceedings, Annual Conference Series*, pages 111–120, Aug. 1999.

[20] D. Zorin and P. Schröder. Subdivision for modeling and animation. In *SIGGRAPH 2000 Course Notes*, 2000.

[19] D. Zorin. Smoothness of stationary subdivision on irregular meshes. *Constructive Approximation*, 16:359–398, 2000.

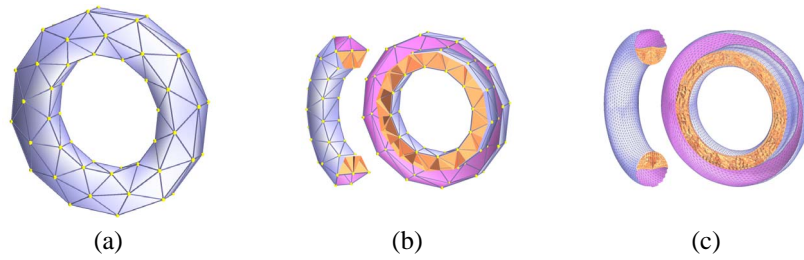


Figure 17. A torus model with non-manifold topology. (a) The original control points. (b) Cross-sections of the control points. (c) Cross-sections of the model at level 4. The purple region indicates the part of the model where only surface information is offered.

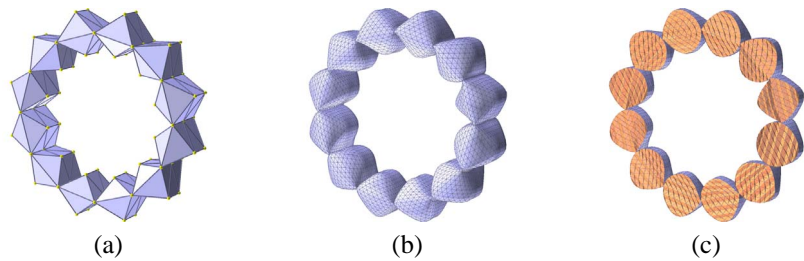


Figure 18. A segmented ring model. (a) The original control points. Each segment meets at a line which forms a non-manifold. (b) The boundary of the model at level 4. (c) A cross-section of the model at level 4.

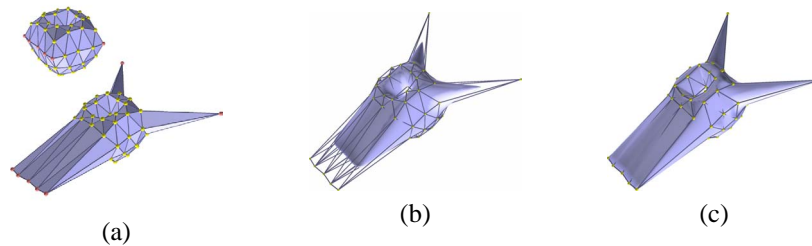


Figure 19. A direct manipulation on control points. (a) The original control points and their modification by a user. (b) The shape generated using an approximate scheme. (c) The interpolatory scheme case. The changes on the model are more interactive and intuitive.